Preparation of spherical $LiNi_{0.5}Mn_{1.5}O_4$ with core-multilayer shells structure by co-precipitation method and long cycle performance

Guo-Jiang Zhou [1*], Tao Yu [2], Yang Zhou [3], Li-Guo Wei [1]
[1] Heilongjiang Institute of Science and Technology, College of Environment and Chemical Engineering, NO. 2468 Puyuan Road, Harbin, 150022 China.
[2] Sinopec Shengli Petroleum Engineering Co., Ltd, No. 125, Jinan Road, Dongying, 257002 China.
[3] Heilongjiang Institute of Energy and Environment, No. 15, Songshan Road, Harbin, 150000 China.

Abstract. As a promising cathode material for lithium ion battemensionalry of high voltage, spinel $LiNi_{0.5}Mn_{1.5}O_4$ has attracted interest due to its high discharging voltage at 4.7 V and high energy density of 610 Wh kg^{-1}. In this work, $LiNi_{0.5}Mn_{1.5}O_4$ with a new core-multilayer shells structure (LNMO-900) is synthesized successfully by co-precipitation method and shows a better electrochemical performance. The formation of the core-multilayer shells structure is related to the kirkendall effect, the shell maintains structural stability, and improves long cycle performance. Core-multilayer shells structure is also beneficial for transmission of lithium ion, increasing rate performance. The effects of sintering temperature on the performance of LNMO were further investigated. Core-multilayer shells $LiNi_{0.5}Mn_{1.5}O_4$ is synthesized successfully at 900 ºC for 12 h uniquely. From the integral calculation of XPS spectra, a higher content of Mn^{4+} is observed in the outer shell of LNMO-900 compared with other homogeneous solid particles. The discharge specific capacity of LNMO-900 is 129.3 mAh g^{-1} at 1 C which is superior to others, and after 1000 cycles, LNMO-900 shows capacity retention of 87.9%. The initial capacity of LNMO-900 is 104.9 mAh g^{-1} at 5 C.

1.Introduction

Lithium-ion batteries are widely used as secondary batteries because of their high energy density, long cycle life and environmental friendliness for electrochemistry fields. Spinel LiNi0.5Mn1.5O4 as cathode material of lithium-ion batteries has a theoretical discharge capacity of 146.7 mAh g-1. LiNi0.5Mn1.5O4 is better than other commercial cathode materials in terms of energy density, safety and production cost in materials science fields[1]. LiNi0.5Mn1.5O4 has three-dimensional lithium ion diffusion channels, it has excellent rate performance and can be used in the load-leveling utility application of rapid charge and discharge[2,3]. LiNi0.5Mn1.5O4 cathode material can offer much higher energy density (650 Wh Kg-1) than other cathode material, such as LiCoO2 (540 Wh Kg-1), LiMn2O4 (500 Wh Kg-1) and LiFePO4 (500 Wh Kg-1)[4]. The electrochemical performance can be improved by lattice and surface doping[5]. It can improve performance directly through designing special LiNi0.5Mn1.5O4 structure[6-10].

Various synthesis routes producing $LiNi_{0.5}Mn_{1.5}O_4$ with different morphologies and particle sizes have been reported[11,12]. Changing the transport rate of lithium ion through preparing special structure, thereby improving $LiNi_{0.5}Mn_{1.5}O_4$ electrochemical performance. The intrinsically fast Li^+ diffusion within the three-dimensional spinel structure leads to a good rate capability and cycling stability, making $LiNi_{0.5}Mn_{1.5}O_4$ attractive for vehicle applications[13,14]. Core-multilayer shells structure $LiNi_{0.5}Mn_{1.5}O_4$ has the three-dimensional lithium ion diffusion channels, three-dimensional lithium ion diffusion channels contribute to high capacity, long cycle life and superior rate performance by increasing the contact area of the electrode/electrolyte, exposing a large number of active sites, as well as facilitating electron/Li^+ ions diffusion channel[15-17].

In this work, we have prepared the better performance $LiNi_{0.5}Mn_{1.5}O_4$ with core-multilayer shells structure. Precursor was synthesized from $NiSO_4 \cdot 6H_2O$ and $MnSO_4 \cdot H_2O$ solution. The pH value and the temperature of the solution as well as the droplet acceleration of the two salts should be adjusted[18-21]. Oxygen deficiency during the high temperature calcination will reduce Mn^{4+} to Mn^{3+} in the core[22]. In general, the core can deliver a high capacity, whereas the shell maintains structural stability. $LiNi_{0.5}Mn_{1.5}O_4$ of spherical core-multilayer shells structure is formed by both $Ni_{0.25}Mn_{0.75}CO_3$ and Li_2CO_3 at 900 ºC for 12 h. The formation of the core-multilayer shells structure is related to the kirkendall effect[23]. The valence of Mn is nearly 4+ in the shell and most Mn^{4+} in multilayer shells can maintain the stability of structure. Core-multilayer shells structure can effectively improve the cycling performance of $LiNi_{0.5}Mn_{1.5}O_4$. Compared with other structure of $LiNi_{0.5}Mn_{1.5}O_4$ made from co-precipitation, its cycle capacity retention rate has better advantages[24,25]. $LiNi_{0.5}Mn_{1.5}O_4$ of core-multilayer shells

* Corresponding author: 13089997952@163.com

structure is better than core-single shell and double-shelled hollow structure of $LiNi_{0.5}Mn_{1.5}O_4$ in some electrochemical performances[26,27].

$LiNi_{0.5}Mn_{1.5}O_4$ with a new core-multilayer shells structure was synthesized successfully. Then the effects of sintering temperature on the performance of LNMO were further investigated. In all samples, the sample calcined at 900 ºC with core-multilayer shells structure is the most obvious and the performance is the best. The initial capacity of LNMO-900 is 129.3 mAh g^{-1} at 1 C, which can retain 87.9% capacity retention after 1000 cycles. The initial capacity of LNMO-900 is 104.9 mAh g^{-1} at 5 C.

2.Materials and Methods

2.1.Characterization and Preparation of $LiNi_{0.5}Mn_{1.5}O_4$

All reagents were analytical grade without further purification. NiSO4 · 6H2O (0.5 mol/L) and MnSO4· H2O (1.5 mol/L) were dissolved evenly in deionized water at a molar ratio Ni: Mn = 1: 3 stoichiometric ratio. Na2CO3 (2 mol/L) was dissolved in deionized water evenly. And appropriate amount of NH3·H2O (25%) was added to the Na2CO3 solution. A four-necked flask with 300 mL deionized water and NaHCO3 (0.03 mol/L) were placed in a constant temperature water bath (55 oC). The sulfate solution and Na2CO3 solution were dumped into the four-neck flask by peristaltic pump at rate of 30 drops per minute and 25 drops per minute respectively. The continuous reaction was controlled at 55 oC and a constant pH of 7.6. After the complete addition of sulfate, the temperature of water bath was increased to 60 oC and a stirring speed of 1200 rpm/min to obtain carbonate precursor (Ni0.25Mn0.75CO3). The obtained precursors were washed with deionized water and then dried at 120 oC. Finally the prepared precursor was mixed thoroughly with appropriate amount Li2CO3. Mixture was sintered at 500 oC for 6 h with subsequent sintering by 850, 900 and 950 oC respectively for 12 h. They were labeled LNMO-850, LNMO-900, LNMO-950, respectively.

The surface images and energy dispersive spectrometer of the powders were captured by Scanning Electron Microscope (SEM) (PHENOM, Phenom Pro X, China) with an accelerating voltage of 25 kV. Powder X-ray diffraction (XRD) measurement is performed to identify crystal structures of the materials on a Rigaku MutiFlex Diffractometer (D/max-2500, Japan) using Cu Kα-radiation at 20 kV and 4 mA. The scanning range of 2θ is from 10° to 80°. X-ray photoelectron spectroscopy (XPS) measurement were captured by Thermo Scientific Escalab Xi+. X-ray photoelectron spectroscopy were used to observe the particle valence changes. The C 1s peak of 284.6 eV was used as a reference to correct all bonding energies.

2.2.Electrochemical measurements

To prepare working electrodes, the prepared samples, Super P and a binding agent (PVDF) were mixed evenly with a ratio of 8: 1: 1. It was uniformly coated on an aluminum foil and then dried at 120 oC for 12 h in a vacuum. Finally, punching it into a 10 mm diameter disk to form working electrodes, the mass loading of active materials is about 2.37 mg/cm2. Assembly work was carried out in an argon-filled glove box, and all prepared electrodes and lithium electrodes were installed into CR2025 button cells for later electrochemical testing. The electrolyte was 1 mol/L LiPF6 solution with ethylene carbonate and diethyl carbonate in a 1:1 volume ratio as a solvent. A LAND BTS automatic battery test system (Shenzhen Xinwei Electronics Co, Ltd) is used for charging/discharging. The cells were activated by constant current charging /discharging after 3 cycles at 0.2 C (1 C=146.7 mA g-1) and cycling performance was tested at 1 C. Cyclic voltammetry (CV) and EIS were performed on a CHI650D Electrochemical Workstation (Shanghai Chenhua Instruments Co., Ltd). CV tests were recorded at 2.0-4.8 V with a scanning rate of 0.1 mV/s. EIS tests of all samples adopted a range of frequency from 0.01Hz to 100 kHz.

3.Results & Discussion

XRD of LiNi0.5Mn1.5O4 at different calcination temperature are shown in Fig. 1. According to the standard XRD-PDF card, XRD of the samples are matched with the cubic spinel LiNi0.5Mn1.5O4 (JCPDS: 80-2162). It can be seen that there are weak impurity peaks at 37.5°, 43.5° and 67.3°. These impurity peaks correspond to LixNi1-yO[28,29], which is a common impurity in LiNi0.5Mn1.5O4 materials. From Fig. 1, it can be seen that the samples are almostly pure spinel LiNi0.5Mn1.5O4.

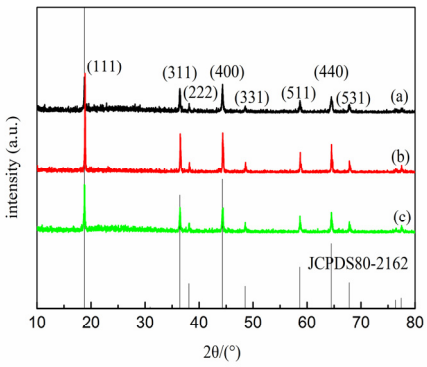

Fig. 1. X-ray diffraction patterns of $LiNi_{0.5}Mn_{1.5}O_4$: (a) LNMO-850; (b) LNMO-900; (c) LNMO-950.

The SEM photographs of Ni0.25Mn0.75CO3 precursor microspheres are exhibited in Fig. 2a-c. It can observe directly the structure of the Ni0.25Mn0.75CO3 precursor and its cathode material of spherial structure. The spherical structure of LiNi0.5Mn1.5O4 maintains the spherical structure of carbonate precursor.

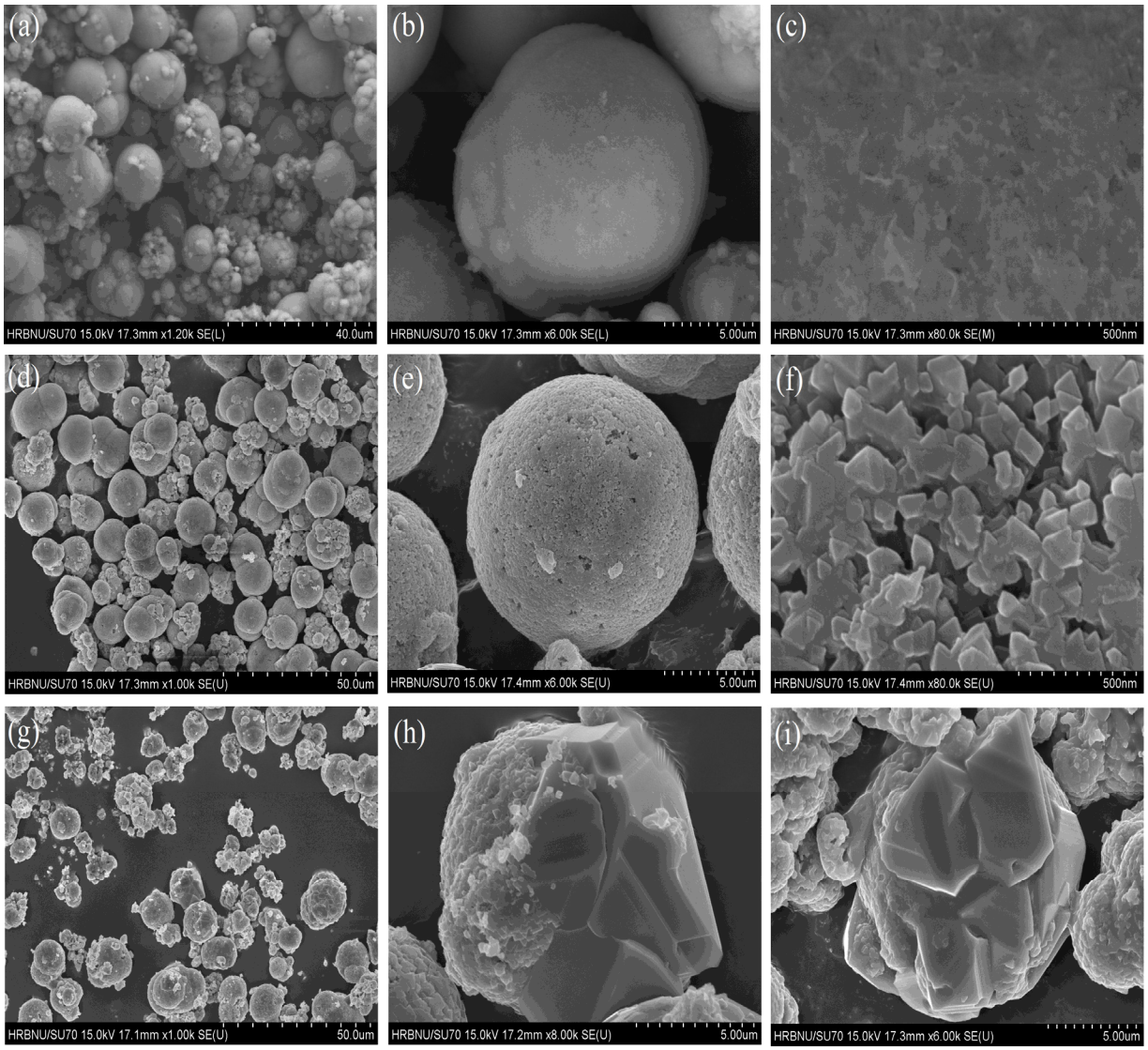

Fig. 2. (a), (b), (c): SEM images of $Ni_{0.25}Mn_{0.75}CO_3$ microspheres, the inset shows the outer surface of the microsphere; (d), (e) SEM image of LNMO-850; (f) a high magnification 500 nm SEM image of LNMO-850 surface morphology; (g), (h), (i) SEM image of LNMO-950 microsphere.

Fig. 2 displays the SEM of LiNi0.5Mn1.5O4 at 850 oC and 950 oC. The LiNi0.5Mn1.5O4 particle size is about 6 μm in Fig. 2e, retaining the porous spherical structure of Ni0.25Mn0.75CO3. There are some holes in the shell of the product, which are probably caused by the emission of CO2 gas during the calcination process. These pores can serve as channels for electrolyte penetration, which is beneficial for the reduction of internal resistance and improving rate capability for lithium ion batteries. The primary spinel of LNMO-850 are small and irregular in Fig. 2f, which length is about 100 nm. The SEM photographs of LNMO-950 is exhibited in Fig. 2g-i. As the temperature of calcination rises, primary particles begin to agglomerate into large spinel of polyhedrons, microsphere begin to agglomerate into polyhedrons and the core-multilayer shells structure disappear gradually. Fig. 2g-i show two morphologies for LNMO-950, it contains two kinds of particles, microsphere and polyhedron. Because the calcination temperature is high, primary spinel particle of microsphere crystallizes to big particle, sphere structure crystallize to polyhedron morphology.

The spherical structure of LNMO-850 is not core-multilayer shells structure. As the calcination temperature rises from 850 oC to 900 oC, the crystallinity of small spinel particles grows larger, and the core-multilayer shells structure is formed. The primary LiNi0.5Mn1.5O4 particles in Fig. 3b has more regular spinel morphology, the microsphere with core-multilayer shells structure is more obvious. The LNMO-900 in Fig. 3a-c are spherical core-multilayer shells structure, in which the inner and outer shells are composed of spinel with a size of 200-400 nm.

EDS mapping of Fig. 3 is performed to analyze the composition of element for LNMO-900. Ni and Mn are distributed uniformly in both core and shell, indicating that core and shell in LNMO-900 have the same chemical formation. The EDS results perform on the cross-section of single microsphere, it confirms further that the microsphere of LNMO-900 contain Mn and Ni.

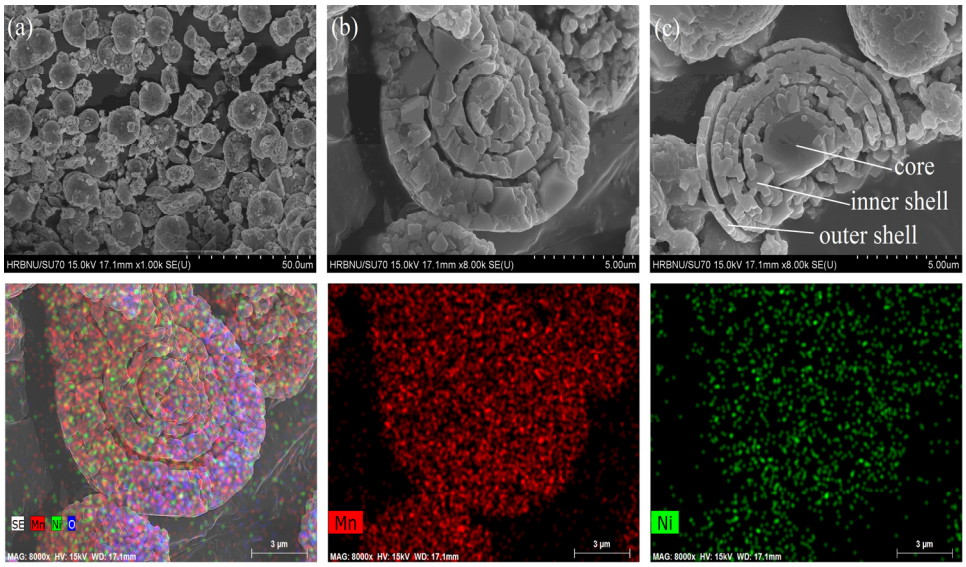

Fig. 3. (a), (b), (c): SEM image of LNMO-900 microsphere, the core, inner shell and outer shell are indicated. EDS mapping of Mn and Ni of LNMO-900 for core-multilayer structure.

We design and prepare core-multilayer shells microspheres of LiNi0.5Mn1.5O4 using Ni0.25Mn0.75CO3 microspheres as self-templates without any additional templates or surfactants[30,31]. The nano-building blocks with short diffusion distance facilitate the Li+ ions rapid diffusion, and the porous structure allows penetration of the electrolyte into the whole microspheres, both contributing to better rate capability. The void and space between the inner and outer shells can buffer against volume changes during Li+ ions insertion/extraction processes, alleviate the problem of pulverization and reduces the charge transfer resistance (Rct), leading to the improved long-term cycling stability[24,32].

XPS spectra of Mn 2p, Ni 2p, C 1s and Li 1s are collected to further research the impact of the valence of manganese ion in the electronic environment. Fig. 4 displays the survey spectra of the samples, and the clear peak of Mn 2p in Fig. 5 further proves the maximum Mn4+ in the shell of LNMO-900. Mn2+ in the precursor outer shell of LiNi0.5Mn1.5O4 is oxidized to Mn4+, Mn2+ in the core will be oxidized to Mn3+ and core contains Mn3+ which improves the discharge specific capacity of the LiNi0.5Mn1.5O4.

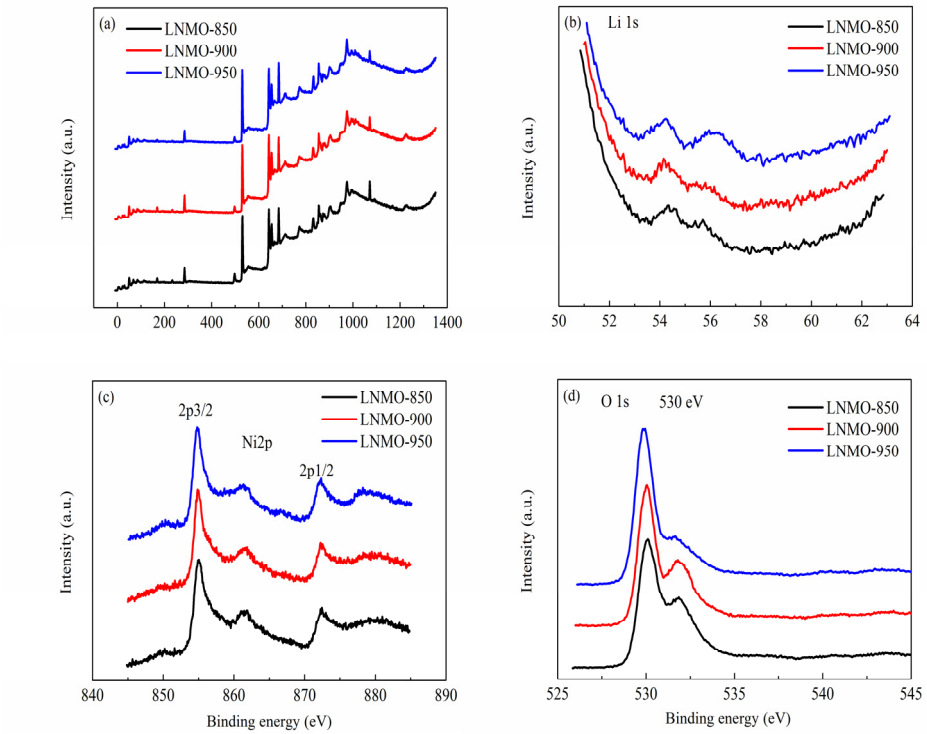

Fig. 4. XPS spectra of LNMO-850, LNMO-900 and LNMO-950: (a) XPS survey, (b) Li 1s, (c) Ni 2p, (d) O 1s.

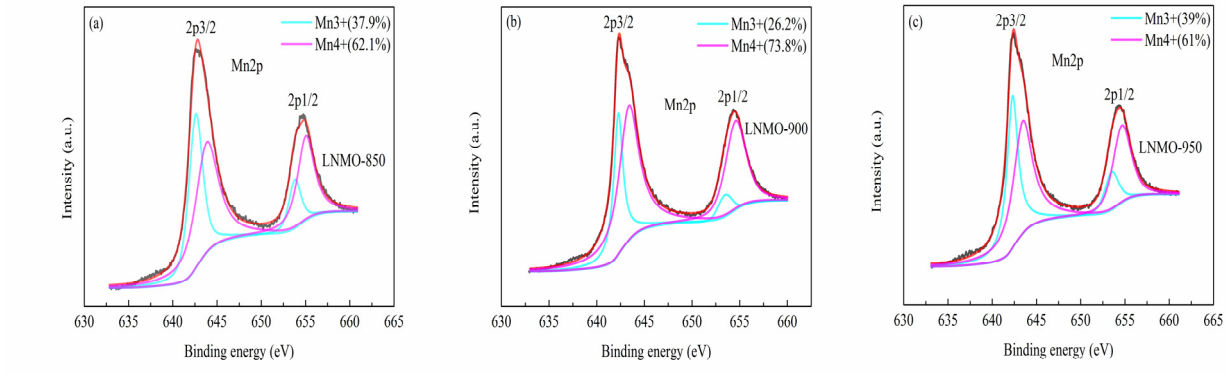

Fig. 5. XPS spectra and fitting results of survey for Mn 2p: (a) LNMO-850, (b) LNMO-900, (c) LNMO-950.

XPS spectra indicates that spectra of LiNi0.5Mn1.5O4 do not increase the intensity of peak and shift the position of electron binding energy except for spectra of Mn. It is further proved that the content of manganese ions with different valence in the shell has a significant effect on the electrochemical properties of the material. The integral calculation gives the contents of Mn4+(Mn3+) as 62.1%(37.9%) for LNMO-850, Mn4+(Mn3+) as 73.8%(26.2%) for LNMO-900 and Mn4+(Mn3+) as 61%(39%) for LNMO-950 in Fig. 5. This indicates that different calcination temperature acts on the electronic environment of the surface structure of the particles. Fig. 5 indicates that shell of LNMO-900 contains the most Mn4+, LNMO-900 with core-multilayer shells structure which keeps the large amount of internal Mn3+ and the higher discharge specific capacity. The shell contains the most Mn4+ which reduce the Jahn-Teller effect of Mn3+, this also suppressing structural damage[26,27], therefore maintain a high cycle capacity retention rate. XPS spectra indicate that valence of oxygen is - 2 valence, lithium is + 1 valence, and nickel is + 2 valence. The valence of manganese for all samples include + 3 valence and + 4 valence, and the average valence state of manganese is below + 4 valence, so there is oxygen defect in spinel crystal structure. Thereby also improving the discharge specific capacity effectively.

Initial charge/discharge profile of LiNi0.5Mn1.5O4 at 1 C are tested in Fig. 6a. The discharge specific capacities of LNMO-850, LNMO-900 and LNMO-950 are 128.8 mAh g-1, 129.3 mAh g-1 and 128.6 mAh g-1 respectively.

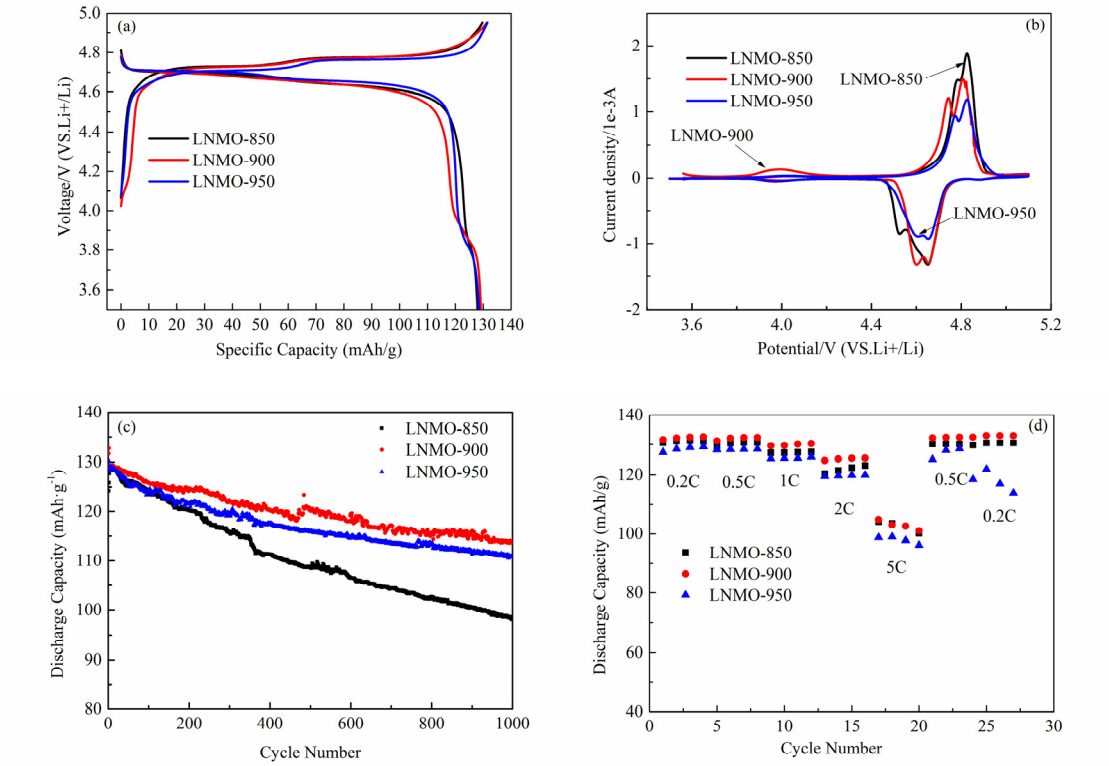

Fig. 6. (a) initial charge/discharge profile of LNMO-850, LNMO-900 and LNMO-950 at 1C; (b) CV of different samples; (c) cycle performances of different samples at 1 C; (d) rate performance of different samples for increasing rates of 0.2, 0.5, 1, 2, 5 C.

As can be seen from Fig. 6a, the discharge capacity for all samples appears on the discharge platform of 4.7 V potential (vs. Li+/Li), which corresponds to Ni4+/Ni3+, Ni3+/Ni2+ redox pairs[33]. In Fig. 6a, there

is an apparent discharge platform of 4.0 V potential (vs. Li+/Li), this platform is due to the reaction of Mn4+ to Mn3+, the discharge platform near 4.0 V can qualitatively analyze the content of Mn3+ in LiNi0.5Mn1.5O4[34]. Fig. 6a shows that LNMO-900 has a relatively long 4.0 V potential platform, indicating that LNMO-900 contains more Mn3+ resulting from oxygen defect. The discharge capacity of LNMO-900 is the highest at 1 C, and the initial discharge capacity is 129.3 mAh/g. Fig. 6b shows cyclic voltammetry curves at different calcination temperature. All samples have an obvious current peak near 4.7 V, which corresponds to Ni4+/Ni3+ and Ni3+/Ni2+ redox pairs. There is a weak current peak at 4.0 V, which corresponds to the redox pair of Mn4+/Mn3+[35], the current peak is formed at the 8a position of Li+ embedded in Fd3m LiNi0.5Mn1.5O4 of spinel octahedron, it results in area of 4.0 V peak[36]. 4.0 V peak area shows that core of LNMO-900 has the more Mn3+.

Fig. 6c displays a cycle performance curve for 1000 cycles at different calcination temperature. All samples are activated by 0.2 C after three cycles and then tested at 1 C condition. It can be seen from the Fig. 6c that LiNi0.5Mn1.5O4 synthesized by co-precipitation has a high cyclic capacity retention rate. The discharge specific capacities of LNMO-850, LNMO-900 and LNMO-950 in the first cycle at 1 C are 128.8 mAh g-1, 129.3 mAh g-1 and 128.6 mAh g-1 respectively. The discharge specific capacities after 1000 cycles are 98.2 mAh g-1, 113.7 mAh g-1 and 110.9 mAh g-1 respectively, the capacity retention rates are 76.2%, 87.9% and 86.2%. The 1 C capacity of LNMO-900 is the highest.

XPS specrte of Mn 2p indicates that outer shell surface of LNMO-900 contains the most Mn4+. Shell of LNMO-900 has the most Mn4+ after high temperature calcination, which can better alleviate structure corrosion during high voltage charge-discharge cycle. The spherical LiNi0.5Mn1.5O4 has a high cycle capacity retention rate because the spherical shell have most Mn4+[37,38]. It can be seen that spinel LiNi0.5Mn1.5O4 with core-multilayer shells structure has excellent cyclic capacity retention rate and residual capacity after cycling. The discharge specific capacity of LNMO-900 after 1000 cycles is 113.7 mAh g-1, and the capacity retention rate of LNMO-900 is 87.9%.

LiNi0.5Mn1.5O4 is tested at different rate of 0.2 C to 5 C. As shown in Fig. 6d, with the increasing rate from 0.2 C to 5 C, its discharge capacity decreases gradually. The initial capacity of LNMO-850, LNMO-900 and LNMO-950 are 104.1 mAh g-1, 104.9 mAh g-1 and 98.9 mAh g-1 at 5 C respectively. The 5 C capacity of LNMO-850, LNMO-900 and LNMO-950 are 77%, 76.2% and 74.2% of that 0.2 C respectively. The presence of the void between the hierarchically multilayer shells could serve as a reservoir for the electrolyte and allow much easier penetration of the electrolyte into the inside of the microspheres, thereby resulting in the facilitation of electrochemical insertion/extraction of Li+ and inhibiting the structural damage. The compact solid irregular particles is not beneficial to the transfer speed of lithium ion, LNMO-950 is compact solid structure, there is no good ion transport channel. It results in bad rate performance and large electric charge transfer resistance (Rct)[39]. The capacity of LNMO-950 is the lowest at 5 C.

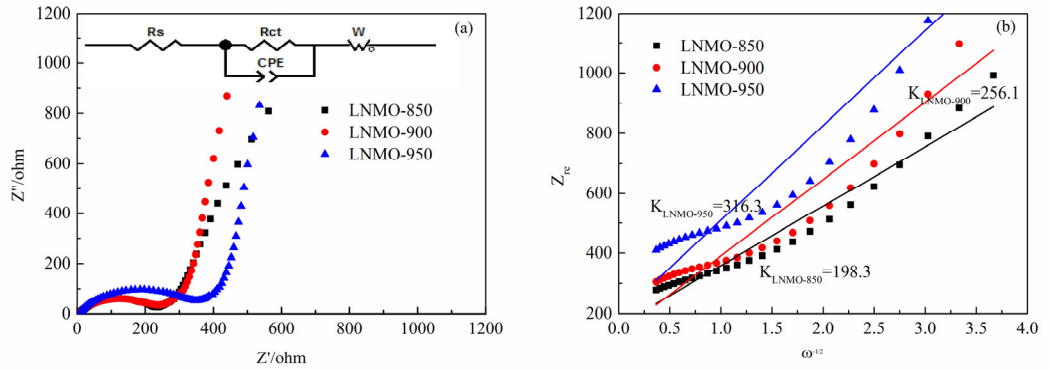

Fig. 7. (a) Nyquist plots of $LiNi_{0.5}Mn_{1.5}O_4$ after activation of three cycles and equivalent circuit used to fit the EIS; (b) Z_{re}-$\omega^{-1/2}$ relation of $LiNi_{0.5}Mn_{1.5}O_4$ material in Low frequency zone.

Fig. 7 shows the electrochemical impedance spectra of all samples and Zre-ω-1/2 relation of LiNi0.5Mn1.5O4 in Low frequency zone. Table 1 shows the parameters of EIS data that are fitted by Zview and Li+ diffusion coefficient. Li+ diffusion coefficient is based on the following formula[40]:

$$D_{Li+} = \frac{R^2T^2}{2A^2n^4F^4(C_{Li})^2\sigma^2}$$

Table 1 Electric charge transfer resistance (R_{ct}) and Li^+ diffusion coefficient (D_{Li+}) of $LiNi_{0.5}Mn_{1.5}O_4$.

samples	R_{ct} / Ω (after activation)	D_{Li+} / $cm^{-2}\cdot s^{-1}$(after activation)
LNMO-850	235.3	$4.11532x10^{-17}$
LNMO-900	211	$2.46735x10^{-17}$
LNMO-950	310.3	$2.27682x10^{-17}$

The electric charge transfer resistance (Rct) of LNMO-900 is fewer than that of LNMO-850 and LNMO-950. Firstly, core-multilayer shells structure of LNMO-900 has a better three-dimensional lithium-ion diffusion path, three-dimensional lithium-ion diffusion path indicates that lithium ions can diffuse through

multiple paths and not just surface lithium layer. Secondly, XPS spectra of Mn 2p shows the absence of oxygen element in LNMO-900. The oxygen defect in spinel can cause oxygen defect in crystal lattice, resulting in oxygen defect. Oxygen vacancy is filled by electrons which conductivity is higher than that of ions, the oxygen defect in spinel helps lithium ion diffusion. Two advantages of spinel morphology for LiNi0.5Mn1.5O4 can increase the diffusion coefficient of lithium ions and reduce electric charge transfer resistance (Rct). A variety of conditions are known to alter the transition metal oxidation state, such as the generation of oxygen vacancies[41-43]. The crystallinity of LNMO-850 is not enough large, the primary spinel is too small to form core-multilayer shells, so the electrochemical impedance of LNMO-850 is higher than that of LNMO-900. LNMO-950 particles aggregate into spinel of polyhedral without multilayer shells structure. Large polyhedral spinel particles without multilayer shells structure increase electrochemical impedance[44-46], large polyhedral spinel particles is against for lithium ion diffusion by decreasing the contact area of the electrode/electrolyte[47]. Multilayer shell structure has a low electrochemical impedance resulting from good diffusion coefficient of lithium ion[48,49]. The electric charge transfer resistance (Rct) of LNMO-900 is the lowest in table 1.

4.Conclusions

In summary, we have successfully designed and synthesized core-multilayer shells microspheres of LiNi0.5Mn1.5O4 using Ni0.25Mn0.75CO3 microspheres as self-templates without any additional surfactants. We prepare LiNi0.5Mn1.5O4 with core-multilayer shells structure, study the particle morphology and electrochemical performance of LiNi0.5Mn1.5O4 at different calcination temperature. Core-multilayer shells LiNi0.5Mn1.5O4 is synthesized successfully at 900 oC uniquely, which displays the highest capacity retention rate and the best rate performance. The multilayer shells structure can alleviate structural degradation during insertion/extraction of lithium ion, leading to improved long-term cycling stability. The hierarchical multilayer shells structure has shown potential to enhance electrochemical performance for cathode materials, and design of the core-multilayer shells structure will be a new and effective approach to high-performance electrode materials.

Acknowledgements

Project No. TSTAU- C2018004 supported by Research and Development Project for Scientific and Technological Achievements of Provincial Universities of Heilongjiang Education Department (NO. TSTAU-C2018004).

Compliance with ethical standards

Conflict of interest The authors declare that they have no conflicts of interest.

References

1. Yi T F, Mei J, Zhu Y R. (2016) Key strategies for enhancing the cycling stability and rate capacity of $LiNi_{0.5}Mn_{1.5}O_4$ as high-voltage cathode materials for high power lithium-ion batteries[J]. J Power Sources 316: 85-105.
2. Yi T F, Fang Z K, et al. (2014) Synthesis of $LiNi_{0.5}Mn_{1.5}O_4$ cathode with excellent fast charge-discharge performance for lithium-ion battery[J]. Electrochim Acta 147:250-256.
3. Wang I D, Choi D, et al. (2009) Self-assembled TiO_2 graphene hybrid nanostructures for enhanced Li-Ion[J]. ACS Nano 3(4): 907-914.
4. M, Armand, J-M, et al. (2008) Building better batteries.[J]. Nature.
5. Zhong G B, Wang Y Y, Zhang Z C, et al. (2011) Effects of Al substitution for Ni and Mn on the electrochemical properties of $LiNi_{0.5}Mn_{1.5}O_4$[J]. Electrochim acta, 56(18):6554-6561.
6. J.-H. Kim, S.-T. Myung, C. S. Yoon, et al. (2004) Comparative study of $LiNi_{0.5}Mn_{1.5}O_{4-\delta}$ and $LiNi_{0.5}Mn_{1.5}O_4$ cathodes having two crystallographic structures: Fd3m and $P4_332$[J]. Chemistry of Materials, 16(21):906-914.
7. Kunduraci M, Amatucci G G. (2008) The effect of particle size and morphology on the rate capability of 4.7 V $LiMn_{1.5+\delta}Ni_{0.5-\delta}O_4$ spinel lithium-ion battery cathodes[J]. electrochimica acta, 53(12):4193-4199.
8. Zhu Z, Yan H, Zhang D, et al. (2013) Preparation of 4.7 V cathode material $LiNi_{0.5}Mn_{1.5}O_4$ by an oxalic acid-pretreated solid-state method for lithium-ion secondary battery[J]. Journal of power sources, 224(Feb.15):13-19.
9. J. B. Fei, Y. Cui, X. H. Yan, et al. (2010) Controlled preparation of MnO_2 hierarchical hollow nanostructures and their application in water treatment [J]. Advanced Materials, 20(3):452-456.
10. Cuizhi Y L, Sun Z, Zhuang Q C. (2011) Electrochemical properties of a 4.7 V-class $LiNi_{0.5}Mn_{1.5}O_4$ positive electrode material for gigh power Li-ion battery[J]. Journal of Inorganic and Organometallic Polymers and Materials, 21(4):893-899.
11. Boyano I, Blazquez J A, Meatza I D, et al. (2010) Preparation of C-$LiFePO_4$/polypyrrole lithium rechargeable cathode by consecutive potential steps electrodeposition[J]. Journal of power sources, 195(16):p.5351-5359.
12. Chi L H, Dinh N N, Brutti S, et al. (2010) Synthesis, characterization and electrochemical properties of 4.8 V $LiNi_{0.5}Mn_{1.5}O_4$ cathode material in lithium-ion batteries[J]. Electrochimica Acta, 55(18):5110-5116.

13. Hwang B J, Wu Y W, Venkateswarlu M, et al. (2009) Influence of synthesis conditions on electrochemical properties of high-voltage $Li_{1.02}Ni_{0.5}Mn_{1.5}O_4$ spinel cathode material[J]. Journal of Power Sources, 193(2):828-833.
14. Yi T F, Xie Y, Ye M F, et al. (2011) Recent developments in the doping of $LiNi_{0.5}Mn_{1.5}O_4$ cathode material for 5 V lithium-ion batteries[J]. ionics, 17(5):383-389.
15. Zhu Y Q, Cao T, Li Z, et al. (2018) Two-dimensional SnO_2/graphene heterostructures for highly reversible electrochemical lithium storage[J]. Science China Materials, 61: 1527-1535.
16. Chen D, Peng L, Yuan Y, et al. (2017) Two-dimensional holey Co_3O_4 nanosheets for high-rate alkali-ion batteries: From rational synthesis to in situ probing. Nano Lett, 17: 3907–3913.
17. Zhu Y, Cao C. (2015) A simple synthesis of two-dimensional ultrathin nickel cobaltite nanosheets for electrochemical lithium storage. Electrochim Acta, 176: 141–148.
18. Zhu Z, Qi lu, et al. (2014) Preparation of spherical hierarchical $LiNi_{0.5}Mn_{1.5}O_4$ with high electrochemical performances by a novel composite co-precipitation method for 5V lithium ion secondary batteries[J]. Electrochim Acta 115: 290-296.
19. S, R, et al. (2013) High precision coulometry study of $LiNi_{0.5}Mn_{1.5}O_4$/Li coin cells[J]. J Electrochem Soc 160(9): A1517-1513.
20. Gu Y J, Zang Q F, et al. (2014) Characterization and electrochemical properties of $LiNi_{0.5}Mn_{1.5}O_4$ prepared by a carbonate Co-precipitation method[J]. Int J Electrochem Sci 9(12):7712-7724.
21. Zhou G J, Yu T, et al. (2020) Effect of carbon nanotubes content on rate performance of spherical $LiNi_{0.5}Mn_{1.5}O_4$ cathode material[J]. Journal of Heilongjiang University of Science and Technology 30(01):71-78.
22. Fauteux D G, Massucco A, et al. (1997) Flexible synthesis of mixed metal oxides illustrated for $LiMn_2O_4$ and $LiCoO_2$[J]. J Appl Electrochem 27(5): 543-549.
23. Zhou L, Zhao D, Lou X W. (2012) $LiNi_{0.5}Mn_{1.5}O_4$ Hollow structures as high-performance cathodes for lithium-ion batteries[J]. Angew Chem Int Ed 51(1): 239-241.
24. Ding Y L, Zhao X B, et al. (2011) Double-shelled hollow microspheres of $LiMn_2O_4$ for high-performance lithium ion batteries[J]. J Mater Chem 21(26): 9475-9479.
25. Lee E, Persson K A. (2013) Solid-solution Li intercalation as a function of cation order/disorder in the high-voltage $Li_xNi_{0.5}Mn_{1.5}O_4$ spinel[J]. Chem Mater 25(14): 2885-2889.
26. Kim J H, Huq A, et al. (2014) Integrated nano-domains of disordered and ordered spinel phases in $LiNi_{0.5}Mn_{1.5}O_4$ for Li-ion batteries[J]. Chem Mater 26(15): 4377-4386.
27. Zhang X, Zheng H, et al. (2011) Flame synthesis of 5 V spinel-$LiNi_{0.5}Mn_{1.5}O_4$ cathode-materials for lithium-ion rechargeable-batteries[J]. P Combust Inst 33(2): 1867-1874.
28. Kim J H, Myung S T, Sun Y K. (2004) Molten salt synthesis of $LiNi_{0.5}Mn_{1.5}O_4$ spinel for 5 v class cathode material of li-ion secondary battery. Electrochim Acta 49(2): 219-227.
29. Menzel M, Schlifke A, et al. (2013) Surface and in-depth characterization of lithium-ion battery cathodes at different cycle states using confocal micro-X-ray fluorescence-X-ray absorption near edge structure analysis[J]. Spectrochim Acta B 85: 62-70.
30. King'ondu, Cecil K, et al. (2011) Light-assisted synthesis of metal oxide hierarchical structures and their catalytic applications[J]. J Am Chem Soc 133(12): 4186-4189.
31. Jin L, Xu L, et al. (2010) Titanium containing γ-MnO_2 (TM) hollow spheres: one-step synthesis and catalytic activities in Li/air batteries and oxidative chemical reactions[J]. Adv Funct Mater 20(19): 3373-3382.
32. Liu H, Wang J, et al. (2016) Morphological evolution of high-voltage spinel $LiNi_{0.5}Mn_{1.5}O_4$ cathode materials for lithium-ion batteries: The critical effects of surface orientations and particle size[J]. ACS Appl Mater Interfaces 8(7): 4661-4675.
33. Santhanam R, Rambabu B. (2010) Research progress in high voltage spinel $LiNi_{0.5}Mn_{1.5}O_4$ material[J]. J Power Sources 195(17): 5442-5451.
34. Xiao J, Chen X, et al. (2012) High-performance $LiNi_{0.5}Mn_{1.5}O_4$ spinel controlled by Mn^{3+} concentration and site disorder[J]. Adv Mater 24(16): 2109-2116.
35. Zhao Q, Ye N, et al. (2010) Oxalate coprecipitation process synthesis of 5 V cathode material $LiNi_{0.5}Mn_{1.5}O_4$ and its performance[J]. Rare Metal Mat Eng 39(10): 1715-1718.
36. Amdouni N, Zaghib K, et al. (2007) Magnetic properties of $LiNi_{0.5}Mn_{1.5}O_4$ spinels prepared by wet chemical methods[J]. J Magn Magn Mater 309(1): 100-105.
37. Rosedhi N D, Idris N H, et al. (2016) Disordered spinel $LiNi_{0.5}Mn_{1.5}O_4$ cathode with improved rate performance for lithium-ion batteries[J]. Electrochim Acta 206: 374-380.
38. Lian F, Zhang F, et al. (2017) Constructing a heterostructural $LiNi_{0.4}Mn_{1.6}O_{4-\delta}$ material from concentration-gradient framework to significantly improve its cycling performance[J]. ACS Appl Mater Inter 9(18): 15822-15829.
39. Kunduraci M, Al-Sharab J F, Amatucci G G. (2006) High-power nanostructured $LiMn_{2-x}Ni_xO_4$ high-voltage lithium-ion battery electrode materials: Electrochemical impact of electronic conductivity

and morphology[J]. Chem. Mater 18(15): 3585-3592.

40. Seyyedhosseinzadeh H, Mahboubi F, Azadmehr A. (2013) Diffusion mechanism of lithium ions in $LiNi_{0.5}Mn_{1.5}O_4$[J]. Electrochim Acta 108: 867-875.
41. Erickson E M, Sclar H, et al. (2017) High-temperature treatment of Li-rich cathode materials with ammonia: improved capacity and mean voltage stability during cycling[J]. Adv Energy Mater 7(18): 708-718.
42. Zhou G J, Yu T, et al. (2019) Effect of calcination temperature on the structure and electrical Properties of $LiNi_{0.5}Mn_{1.5}O_4$ material[J]. Journal of Heilongjiang University of Science and Technology 29(04):424-429.
43. Reed J, Ceder G. (2004) Role of electronic structure in the susceptibility of metastable transition-metal oxide structures to transformation[J]. Chem Rev 104(10): 4513-4534.
44. Goodenough J B, Kim Y. (2010) Cheminform abstract: challenges for rechargeable Li batteries[J]. ChemInform 41(31): 587-603.
45. Liu J, Wang S, et al. (2016) The effect of boron doping on structure and electrochemical performance of lithium-rich layered oxide materials[J]. ACS Appl Mater Inter 8(28): 18008-18017.
46. Zhang Y, Dong P, et al. (2017) Combustion combined with ball milling to produce nanoscale La_2O_3 coated on $LiMn_2O_4$ for optimized Li-ion storage performance at high temperature[J]. J Appl Electrochem 48(2): 135-145.
47. Chong J, Xun S, et al. (2013) Surface stabilized $LiNi_{0.5}Mn_{1.5}O_4$ cathode materials with high-rate capability and long cycle life for lithium ion batteries[J]. Nano Energy 2(2): 283-293.
48. Li L, Xu M, et al. (2015) High-performance lithium-rich layered oxide materials: effects of chelating agents on microstructure and electrochemical properties[J]. Electrochim Acta 174: 446-455.
49. Kumar S, Nayak P K, et al. (2014) Temperature and potential dependence electrochemical impedance studies of $LiMn_2O_4$[J]. J Appl Electrochem 44(1): 61-71.